Journal of Neuroinflammation

RESEARCH

Open Access

Longitudinal accumulation of glial activation measured by TSPO-PET predicts later brain atrophy in multiple sclerosis

Nylund Marjo[1,2,3,4], Lehto Jussi[1,2,4], Matilainen Markus[1,2,3], Rajander Johan[1,5], Wahlroos Saara[1], Sucksdorff Marcus[1,2,3,4], Kuhlmann Tanja[6] and Airas Laura[1,2,3,4*]

Abstract

In multiple sclerosis (MS), accumulation of disability is driven by CNS-compartmentalized inflammation. This inflammatory process involves activated microglia and astrocytes, which contribute to neuroaxonal damage which in turn accelerates disease progression. Activated glial cells express 18-kDa translocator protein (TSPO), and TSPO-binding radioligands and positron emission tomography (PET) imaging can be used to quantitate glial activation in vivo. The aim of this study was to evaluate the longitudinal evolution of glial activation in untreated cohorts of relapsing remitting MS (RRMS) and secondary progressive MS (SPMS) patients over one-year follow-up, and to explore how a change in glial activation associates with later imaging and clinical outcomes. Eighteen untreated MS patients (RRMS $n=8$, SPMS $n=10$) were studied. Expanded disability status scale (EDSS), brain MRI and TSPO-PET scans using [^{11}C]PK11195 were performed at baseline and one year later. Distribution volume ratio (DVR) of [^{11}C]PK11195-binding, and the proportion of TSPO-high voxels at baseline in the normal appearing white matter (NAWM) and other regions of interest were compared to the respective parameters in follow-up scans. Chronic lesions were phenotyped at baseline and at follow-up according to their TSPO-PET-binding patterns, and TSPO-expressing lesions were further characterized using postmortem immunopathological staining. Extended follow-up was obtained after 4–11 years with EDSS available for 18 patients and MR imaging available from 13 patients. TSPO-signal was higher among SPMS compared to RRMS patients at baseline. During one-year follow-up, TSPO uptake remained stable in RRMS patients in all regions of interest. Among the SPMS patients, the proportion of active voxels in the NAWM increased significantly over one-year follow-up. A greater proportion of lesions acquired a rim-active phenotype among SPMS compared to RRMS. According to forward-type stepwise multiple linear regression, change in the proportion of active voxels in the NAWM over one year and baseline body-mass-index were best predictors of later development of brain atrophy ($R2=0.69$). Our study provides novel information about the natural evolution of CNS-compartmentalized inflammation and demonstrates an important link between NAWM TSPO-signal and later adverse outcomes among MS patients, supporting the notion that diffuse glial activation in the NAWM contributes to disease progression.

Keywords Multiple sclerosis, Positron emission tomography, TSPO, Glia, Microglia

*Correspondence:
Airas Laura
laura.airas@utu.fi

Full list of author information is available at the end of the article

Introduction

Multiple sclerosis (MS) is a heterogeneous disease in terms of clinical outcomes [1]. The disease course is driven by diverse underlying pathologies including peripheral activation of adaptive immune cells which enter the central nervous system (CNS) and initiate the formation of focal acute inflammatory infiltrates [2, 3]. An additional CNS-contained glial cell activation process may start early in the disease course and is considered a likely driver of progression independent of relapse activity [3]. The clinical spectrum from benign relapsing remitting (RRMS) to debilitating progressive MS could be partly explained by the severity of the CNS-compartmentalized inflammation [3].

Conventional magnetic resonance imaging (MRI) performs well in capturing signs of focal inflammation, either as acute contrast-enhancing T1 lesions or new/enlarging T2 lesions, but conventional MRI has limited applicability in quantitating the widespread glial cell activation in the CNS [4]. The glial cell-driven CNS inflammatory burden is however quantifiable in vivo with positron emission tomography (PET)-imaging and radioligands that bind to the 18-kDa translocator protein (TSPO). TSPO is expressed in the brain mainly on the outer mitochondrial membrane of activated microglia, macrophages and astrocytes [5]. Following signals of tissue damage or inflammation, the glial cells and immune cells gather densely at the site of injury [6], and this can be captured using TSPO-PET imaging [7]. Of the TSPO-ligands, [^{11}C]PK11195 has been used most extensively in PET imaging of people with MS [8]. TSPO-PET-measurable innate immune cell activation in the normal appearing white matter (NAWM) [9], in the thalamus [10], and in association with chronic focal lesions predicts later MS disease progression [5, 7, 11]. It has been hypothesized that reversing pro-inflammatory microglial activation is beneficial for slowing down disease progression, and microglia-associated inflammation is being currently investigated as a therapeutic target in progressive MS [12]. PET imaging is presently the only in vivo tool to detect dynamic longitudinal changes in the glial cell activation within the CNS [13, 14], but longitudinal studies particularly in untreated MS cohorts are missing and the evolution and kinetics in alteration of glial activation are not well understood.

In an effort to unfold the association between clinical and radiological correlates and the kinetics of alteration in glial cell activation, we conducted a longitudinal study comparing a benign cohort of untreated 'silent' RRMS patients to a cohort of secondary progressive (SPMS) patients with accruing disability. We performed longitudinal TSPO-PET-imaging at one-year interval in these two cohorts and assessed changes in glial activation both in association with chronic lesions and in the NAWM across both groups. Furthermore, characteristics of TSPO-expressing chronic lesions were further analyzed using immunopathological staining of postmortem MS brain. Finally, we evaluated the associations between the early imaging parameters and subsequent clinical disease worsening or brain volume loss evaluated after an extended follow-up of 4–11 years.

Methods

Subjects and procedures

The study cohort consisted of 18 patients with multiple sclerosis (8 with RRMS and 10 with SPMS) who underwent neurological assessment including disability evaluation using expanded disability status scale (EDSS), brain 3T-MR and TSPO-PET imaging at baseline and at one-year follow-up. Extended follow-up data were collected 4–11 years (mean 7, SD 2) after the baseline, with EDSS scores available from all 18 patients and MRI data from 13 patients (7 with RRMS and 6 with SPMS). 18 age-and sex-matched HCs were imaged for comparison at baseline using both TSPO-PET and MRI with similar protocols as patients with MS.

The study was performed at the Turku University Hospital Neurocenter and Turku PET Centre. Inclusion criteria were a confirmed MS diagnosis and no topical disease modifying therapy. Recruitment took place between Jun 2012 and Dec 2020. Key exclusion criteria included pregnancy, claustrophobia, and other significant CNS pathology besides MS. Information on the patient past and current disease activity and treatment history were collected from the patient record system of the Turku University Hospital. Confirmed disability progression was defined as EDSS increase of 1.0 point if baseline EDSS was ≤ 5.5, or EDSS increase of 0.5 point if baseline EDSS was ≥ 6.0 [15]. In all cases the EDSS evaluation for progression was confirmed by re-evaluation after 6 months.

The study protocol was approved by the Ethics Committee of the Hospital District of Southwest Finland. Written informed consent was obtained from all participants according to the principles of the Declaration of Helsinki.

MR image acquisition and processing

To acquire brain volumetric measurements and anatomical references for the PET images, a 3T-MRI (Philips Ingenia/Philips Ingenuity, Best, The Netherlands) with the following sequences: 3D-T1, T2 and 3D fluid-attenuated inversion recovery (FLAIR). All MR images of a given subject from baseline and follow-up time points were co-registered with the respective baseline T1 image using statistical parametric mapping (SPM8, Wellcome Trust Center for Neuroimaging, London, UK).

Intracranial volume (ICV) was calculated in SPM12 (Wellcome Trust Center for Neuroimaging, London, UK)

as sum of grey matter (GM), white matter (WM) and CSF using > 0.9 probability threshold. Region of interest (ROI) masks for T1- and T2-lesions were obtained by first creating an initial mask using LST lesion segmentation tool [16] in SPM12, and thereafter by manually correcting the mask slice by slice in Carimas (Turku PET Centre, Finland) [17]. T1 and T2 lesion volumes were obtained based on these ROI masks.

Whole brain, cerebral WM, cortical GM and thalamic volumes were obtained based on the segmented masks after lesion filling using FreeSurfer (https://surfer.nmr.mgh.harvard.edu/) and compared between the RRMS and SPMS cohorts, and MS and healthy controls (HCs). To estimate glial activation in the NAWM adjacent to lesions, perilesional NAWM mask 3 mm around the T1-lesions was created as described [9]. For lesion phenotyping 2 mm perilesional rim was used [17]. NAWM masks were obtained for volumetric evaluation by subtracting T2-lesion masks from WM masks, and for the NAWM-PET-signal by subtracting the T1-lesion masks dilated by perilesional area (6 mm from the lesion edge) from the WM. Volumes of each ROI were determined as parenchymal fractions (PFs, ROI volume divided by the intracranial volume presented in percentages). The total percentage brain volume change (PBVC) was evaluated using SIENA [18], part of FSL [19] and the annualized atrophy rate was calculated to account for the variation in the follow-up times.

[^{11}C]PK11195 PET acquisition and processing

[^{11}C]PK11195 synthesis has been previously described [20]. Sixty minutes of dynamic list mode PET data was acquired at baseline and after one year with a high-resolution research tomograph (HRRT, Siemens/Control Technology Incorporated, Knoxville, TN) as reported earlier [14].

PET images of each subject were co-registered with the respective baseline T1 image using statistical parametric mapping (SPM8, Wellcome Trust Center for Neuroimaging, London, UK). Image reconstruction [21] and post-processing followed previously described procedures [20]. Specific binding of [^{11}C]PK11195 was quantified as distribution volume ratio (DVR) using Logan's reference tissue model [22] and time-activity curves representing a region without specific binding were acquired with the Matlab (MathWorks Inc.) Super-PK-software [20] and used as the reference time-activity curves. The active voxel threshold was determined by first calculating the mean DVR + 1.96 SD (95% confidence interval) threshold across all cerebral WM voxels for each HC, then computing the group-level mean of these individual values to define the final threshold DVR > 1.56 [17]. Clusters with less than 3 connected voxels were excluded to avoid inclusion of random peak values.

Individual T1-lesions with volume of more than 27mm^3 were classified into inactive, overall-active, and rim-active based on the distribution of active voxels within the lesion core and in the perilesional rim [17]. Rim-active lesions have either less than 5% active voxels in the core with at least 5% points more at the rim, or 5–20% active voxels in the core with at least double that at the rim. Inactive lesions have 0% active voxels in both the core and rim. Overall-active lesions show activity in both regions without a substantial difference between them [17]. For the cohort-wise comparisons presented in Table 1, each individual lesion was analyzed separately. For the longitudinal lesion type analysis presented in Table 3, only lesions existing both at baseline and at the one-year follow-up were analyzed. When two or more lesions grew and fused into a single confluent lesion during the follow-up, the baseline phenotype was determined by combining the corresponding individual lesions into one cohesive lesion.

Immunopathological staining of post-mortem MS brain

One representative active lesion, mixed active and inactive lesion (also termed chronic active lesion) and inactive lesion each were obtained from two donors (1 RRMS and 1 SPMS) from the well characterized MS autopsy cohort collected the Institute of Neuropathology in Münster [6]. Four µm thick formalin fixed and paraffin embedded sections were stained for myelin basic protein (MBP) (Abcam, ab7394, dilution 1: 4000, pretreatment with citrate), HLA-DR (Dako, M077501-2, 1: 100, pretreatment with citrate), GFAP (Dako, Z0334, 1: 4000, no pre-treatment) and TSPO (Invitrogen, MA5-33203, 1:100, no pretreatment). IHC was performed with the Dako REALTM Detection System (#K5001, Dako) and an automatic immunostainer (Autostainer Link 48, Dako) using the biotin–streptavidin method. In brief, tissue sections were deparaffinized and the intrinsic peroxidase activity was blocked by incubation with 5% H_2O_2 in phosphate-buffered saline (PBS). Subsequently, primary antibodies were applied as described above. Species-specific biotinylated mouse, rat, or rabbit antibodies were applied as secondary antibodies and incubated with a streptavidin/peroxidase complex. To complete IHC, the reaction product was developed with diaminobenzidine. For the detection of total (ferric and ferrous) non-heme iron the diaminobenzidine (DAB)-enhanced Turnbull staining was used [23]. Sections were deparaffinized and immersed in 2% aqueous ammoniumsulfide solution for 90 min followed by incubation in an aqueous solution containing 10% potassium ferrocyanide K4[FE(CN)6] and 0.5% hydrochloric acid for 15 min. Sections were washed and incubated in methanol containing 0.3% hydrogen peroxide for 30 min. After washing with PBS pH 7.4, iron staining was amplified by a DAB solution

Table 1 Clinical and imaging variables at baseline in MS cohorts and healthy controls

Variable	HC	MS	RRMS	SPMS	HC vs. MS (*p*-value)	HC vs. RRMS (*p*-value)	HC vs. SPMS (*p*-value)	RRMS vs. SPMS (*p*-value)
n	18	18	8	10				
Follow-up time, months		13.1 (3.0)	13.8 (2.9)	12.6 (3.1)				0.4
Sex, female, n (%)	15 (83)	13 (72)	7 (88)	6 (60)	0.7	1	0.6	0.6
Age, years	45 (7)	46 (9)	42 (7)	50 (9)	0.7	0.6	0.5	0.4
BMI, median (IQR)	24.6 (22.7–26.6)	22.9 (20.0–25.0)	23.0 (22.8–25.6)	22.1 (19.3–23.2)	0.12	0.7	0.19	0.7
Radiation dose (MBq), median (IQR)	496 (482–499)	484 (474–494)	480 (474–494)	484 (466–496)	0.17	0.3	1	1
Time from first symptoms, years, median (IQR)		16 (10–20)	14 (10–19)	18 (12–20)				0.6
Time since last relapse, years, median (IQR)		5.0 (1.7–7.1)	6.8 (2.2–9.2)	4.3 (1.7–5.6)				0.3
EDSS, median (IQR)		3.8 (3–6)	2.8 (1–3.1)	6 (4.3–6)				**0.001**
ARR, median (IQR)		0.23 (0.20–0.40)	0.23 (0.19–0.34)	0.26 (0.21–0.41)				0.8
T2 lesion volume (cm^3), median (IQR)		13.5 (5.9–21.3)	6.1 (2.9–9.1)	20.2 (14.3–39.7)				**0.009**
T1 lesion volume (cm^3), median (IQR)		8.0 (3.9–12.3)	4.0 (2.1-6.0)	12.0 (9.1–27.2)				**0.009**
Brain volume (PF%)	86.7 (2.7)	81.6 (4.8)	83.8 (2.6)	79.8 (5.5)	**< 0.001**	**0.044**	**0.004**	0.12
NAWM volume (PF%)	35.6 (2.6)	31.3 (3.3)	33.0 (2.2)	30.0 (3.5)	**< 0.001**	**0.032**	**< 0.001**	**0.034**
Cortical GM volume (PF%)	33.1 (1.9)	31.2 (2.9)	31.9 (1.6)	30.6 (3.6)	**0.019**	0.18	0.12	0.4
Thalamus volume (PF%)	1.19 (0.12)	0.92 (0.13)	1.01 (0.11)	0.84 (0.11)	**< 0.001**	**0.002**	**< 0.001**	**0.003**
NAWM DVR	1.17 (0.04)	1.23 (0.06)	1.19 (0.03)	1.27 (0.06)	**0.005**	0.4	**< 0.001**	**0.009**
Thalamus DVR	1.28 (0.06)	1.35 (0.10)	1.30 (0.09)	1.38 (0.10)	0.15	0.8	**0.047**	0.2
% of active voxels in NAWM, median (IQR)	5.5 (4.2–7.3)	7.8 (5.8–12.0)	5.8 (4.8–7.3)	11.7 (8.6–14.5)	**0.022**	0.7	**0.003**	**0.031**
% of active voxels in thalamus, median (IQR)	16 (13–23)	20 (13–42)	15 (11–19)	29 (20–46)	0.14	0.7	**0.022**	0.053
Number of[a]								
rim-active lesions, median (IQR)		4 (2–5)	2 (2–4)	4 (3–5)				0.14
overall-active lesions, median (IQR)		13 (7–18)	9 (5–12)	15 (14–20)				**0.040**
inactive lesions, median (IQR)		6 (4–9)	7 (5–8)	5 (4–12)				0.7
Volume of[a]								
rim-active lesions, median (IQR)		0.3 (0.1–0.5)	0.3 (0.06–0.4)	0.4 (0.3-1)				0.2
overall-active lesions, median (IQR)		5 (1–9)	2 (0.9-4)	7 (5–19)				**0.021**
inactive lesions, median (IQR)		0.4 (0.3–0.8)	0.5 (0.4–0.9)	0.4 (0.3–0.7)				0.6

Mean (SD) unless otherwise stated. Differences between the groups have been assessed with Wilcoxon rank-sum test. Holm correction for p-values has been used for variables with all pairwise comparisons HC vs. RRMS, HC vs. SPMS, and RRMS vs. SPMS. [a] Of all lesions > 27 mm^3. ARR = Annualized relapse rate, BMI = body mass index, DVR = Distribution volume ratio, EDSS = Expanded disability status scale, HC = healthy control, IQR = Interquartile range, GM = Grey matter, NAWM = Normal appearing white matter, PF = parenchymal fraction, RRMS = Relapsing remitting multiple sclerosis, SPMS = Secondary progressive multiple sclerosis

(DCS Diagnostics) for 10 min. Afterwards, sections were rinsed in tap water, counterstained with hematoxylin and mounted. The study was approved by the Ethics Committee of the University of Münster (Ref: 2011-153-f-S).

Statistical analysis

All statistical analyses were conducted using R software version 4.4.0 (https://www.r-project.org/about.html). Wilcoxon rank-sum test was used for comparisons between HCs and patients. NAWM and perilesional area DVRs were compared between patients with confirmed disability progression (EDSS change) and no progression (no EDSS change) over time. Wilcoxon signed-rank test was used to compare baseline and follow-up measurements. Holm correction was used for multiple comparisons. Spearman's correlation coefficient was used to assess associations between continuous and ordinal variables.

To compare the effect of changes in different imaging parameters within one-year follow-up on later atrophy at extended follow-up, univariate and forward-type stepwise multivariate linear regression modelling were

performed. Variables with non-normal distribution were log-transformed, including the annualized PBVC. The building of the multivariate model started with no predictors. All imaging variables listed in Table 2 (at baseline or the change from baseline to one year) with a significant Spearman correlation with annualized PBVC, and baseline clinical and demographic variables were considered when the multivariate model was built. Clinical and demographic variables included disease type, gender, age, body mass index (BMI), disease duration, EDSS, and annualized relapse rate (ARR). The first parameter to be added to the model was the one leading to the lowest Akaike information criterion (AIC) value. The second variable added was the one with the lowest AIC value when the first variable was already in the model. Due to the low amount of observations ($n = 13$), the number of predictor variables was restricted to two. Final models were checked for multi-collinearity and influential values. If multicollinearity was present, the variable added later (i.e. variable was not as good as a predictor as the first one) was removed from the considered variables, and the process was run again. Regression coefficients were standardized by multiplying the regression results by twice the SD of studied variable [24]. All tests were two-tailed and a p-value less than 0.05 was considered statistically significant.

Results

Clinical and imaging characteristics of the participants at baseline

18 patients with MS and 18 HCs participated in the study. Eight patients had RRMS, and 10 patients had SPMS. MS patients and HCs had similar age and sex distribution (Table 1). All patients had discontinued DMT utilization on average 15 (range 2–136) months prior to baseline imaging and none of the patients were using DMT during the study. Treatments within one year of study onset: During the year before inclusion one RRMS patient had discontinued glatiramer acetate 2 months before inclusion, and seven RRMS patients had not used a DMT. Among the SPMS cohort, two patients had discontinued interferon beta, one patient had discontinued natalizumab, and one patient had discontinued glatiramer acetate within two to nine months before inclusion. Six patients with SPMS had not used a DMT during the previous year before inclusion. Treatments preceding the year before study onset: Previous treatments among the RRMS cohort included interferon beta (3 patients), dimethyl fumarate (2 patients) and teriflunomide, while the SPMS patients had been earlier treated with mitoxantrone, azathioprine, interferon beta (2 patients), glatiramer acetate, and minocycline. All treatments had been discontinued due to poor perceived tolerability and/or lack of efficacy. Summary of the treatments before baseline are presented in Supplementary Table 1.

At baseline patients with SPMS had smaller NAWM and thalamic volumes compared to RRMS and HCs, and the T1 and T2 lesion volumes were greater among SPMS compared to RRMS (Table 1). Additionally, EDSS scores were significantly higher among SPMS compared to RRMS but there were no significant differences in age or disease duration (Table 1). One SPMS patient had a gadolinium enhancing lesion at the baseline MRI but there were no Gd + lesions at the time of follow-up. The gadolinium enhancing lesion was excluded from the individual lesion phenotype analysis.

Both the [^{11}C]PK11195 radioligand DVR and the proportion of active voxels were higher in the NAWM of SPMS patients compared to RRMS and HCs at baseline (Table 1). No significant differences were observed between RRMS and HC in the NAWM DVR values or the proportion of active voxels. Additionally, higher TSPO-tracer uptake in the NAWM, thalamus and perilesional area all correlated significantly with greater T1 lesion volume and smaller thalamus volume (Fig. 1A-F). Higher EDSS at baseline correlated strongly with greater NAWM DVR (Fig. 1G) and the proportion of active voxels at baseline ($R = 0.52$, $p = 0.025$, data not shown).

Chronic lesion phenotypes based on TSPO-PET-signal and immunohistochemical staining

We performed voxel-based automated phenotyping of lesions based on the analysis of active voxels within the lesion core and at the perilesional rim [17]. Figure 2A demonstrates representative TSPO-PET-based examples of chronic lesion phenotypes rim-active, overall-active and inactive. Figures 2B-D demonstrate neuropathological examples of three MS-lesion subtypes with special reference to TSPO-expression: a mixed-active/inactive lesion, an active lesion and an inactive lesion. Here, mixed-active/inactive lesion shows strong TSPO-staining at the edge of a chronic demyelinated lesion. The TSPO-staining co-localizes with HLA-DR staining for activated microglial cells and with Turnbull staining for the presence of iron. Active and inactive lesions demonstrate TSPO-staining originating not only from HLA-DR-positive active microglia/macrophages, but also from GFAP-positive astrocytes.

At baseline patients with SPMS had a greater number and volume of TSPO-overall-active lesions compared to patients with RRMS (Table 1). Of all T1 hypointense chronic lesions at baseline among RRMS, 14% were rim-active, 47% were overall-active, and 39% were inactive. Among the SPMS the proportions were 15% rim-active; 57% overall-active, and 28% inactive. The differences in the proportions of these different chronic lesion subtypes between RRMS and SPMS patients did not reach

Table 2 Longitudinal changes in clinical and imaging parameters over the one-year follow-up

	RRMS ($n=8$)					SPMS ($n=10$)					Baseline vs. 1-year Follow-up				
	Baseline		1-year follow-up		Baseline vs. 1-year follow-up	Baseline		1-year follow-up		Baseline vs. 1-year follow-up	RRMS change		SPMS Change		RRMS change vs. SPMS change
	Mean	SD	Mean	SD	*p*-value	Mean	SD	Mean	SD	*p*-value	Mean	SD	Mean	SD	*p*-value
NAWM DVR	1.19	0.03	1.19	0.04	0.8	1.27	0.06	1.29	0.05	0.19	0.001	0.031	0.022	0.039	0.3
Thalamus DVR	1.30	0.09	1.31	0.07	0.4	1.38	0.11	1.38	0.12	0.8	0.013	0.038	-0.002	0.036	0.4
T1 hypolesion DVR	1.12	0.09	1.12	0.10	0.8	1.18	0.09	1.19	0.08	0.7	-0.001	0.072	0.012	0.074	0.9
T1 perilesional DVR[a]	1.16	0.06	1.16	0.08	0.9	1.24	0.10	1.25	0.09	0.8	-0.002	0.062	0.029	0.074	0.6
Brain volume (PF%)	83.8	2.6	84.0	2.4	0.5	79.8	5.5	78.5	4.4	0.13	0.24	0.70	-1.33	2.67	0.10
NAWM volume (PF%)	33.0	2.2	33.0	2.1	0.3	30.0	3.5	29.5	4.4	0.064	0.03	0.32	-0.43	0.71	**0.034**
Cortical GM volume (PF%)	31.9	1.6	32.0	1.6	0.6	30.6	3.6	29.8	3.0	**0.027**	0.05	0.38	-0.79	1.46	**0.043**
Thalamus volume (PF%)	1.01	0.11	1.00	0.11	0.5	0.84	0.11	0.81	0.10	**0.010**	-0.00	0.03	-0.31	0.04	0.2
	Median	IQR	Median	IQR	*p*-value	Median	IQR	Median	IQR	*p*-value	Median	IQR	Median	IQR	*p*-value
EDSS	2.8	1–3.1	2.5	1.9–3.1	0.7	6	4.2–6	6	4.2–6.5	0.089	0	-0.1–0.6	0	0–0.5	0.7
T1 hypolesion volume (cm^3)	4.0	2.1–6.0	4.0	2.2–7.3	**0.008**	12.0	9.1–27.2	13.7	9.4–30.0	**0.033**	0.13	0.10–0.39	0.55	0.12–2.98	0.3
T2 lesion volume (cm^3)	6.1	2.9–9.1	6.7	3.2–13.4	**0.008**	20.2	14.3–39.7	24.4	15.3–49.7	**0.002**	0.73	0.22–1.94	2.56	1.34–6.36	0.083
% of active voxels in NAWM	5.8	4.8–7.3	4.9	3.4–7.0	0.9	11.7	8.6–14.5	13.7	11.2–20.3	**0.037**	0.04	-2.5–1.4	4.41	0.06–7.03	0.083
% of active voxels at the rim of T1 lesions[b]	4.6	2.9–5.6	2.8	1.8–6.0	0.7	9	3–16	10	6–15	0.4	-0.6	-2.2–0.6	0.8	-0.7–4.9	0.4

Changes from baseline to follow-up assessed using Wilcoxon signed-rank test. Differences in changes between RRMS and SPMS assessed using Wilcoxon rank-sum test. [a] 0–3 mm from T1 edge, [b] Of all lesions > 27 mm^3. DVR = Distribution volume ratio, EDSS = Expanded Disability Status Scale, GM = Grey matter, IQR = Interquartile range, NAWM = Normal appearing white matter, PF = parenchymal fraction, RRMS = Relapsing remitting multiple sclerosis, SD = Standard deviation, SPMS = Secondary progressive multiple sclerosis

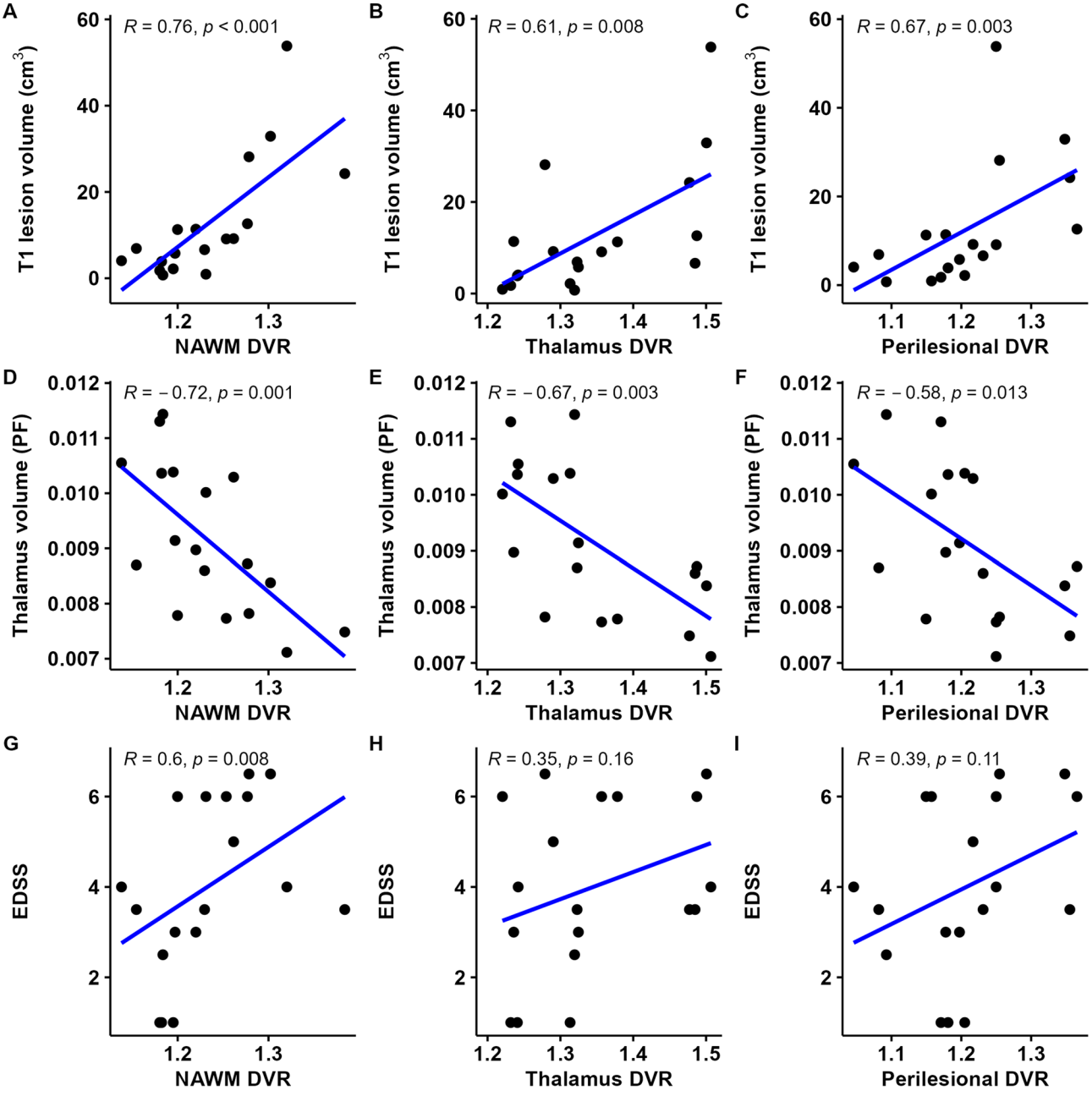

Fig. 1 Correlations between TSPO-availability (DVR) and T1 lesion volume, thalamic volume and EDSS at baseline. Higher TSPO-binding in the NAWM, thalamus and at the perilesional area correlated significantly with higher T1 lesion volume and smaller thalamic volume at baseline (**A**-**F**). NAWM TSPO-binding correlated with EDSS (**G**). Spearman correlation was used for statistical analyses

statistical significance in this small cohort (Fisher test $p = 0.069$).

Changes in brain volumetric measures and TSPO-binding during the one-year follow-up

Cortical GM and thalamic volumes reduced during the one-year follow-up among SPMS patients, while no significant change was observed among the RRMS patients (Table 2). The reduction in the NAWM and cortical GM volumes were of greater magnitude among SPMS patients compared to RRMS (Table 2). Lesion volumes increased among both RRMS and SPMS cohorts during the follow-up (Table 2).

Longitudinal TSPO-uptake remained stable during the follow-up in the RRMS cohort in all regions of interests (Table 2). Among the SPMS patients, the proportion of active voxels in the NAWM increased [median (IQR) 11.7% (8.6–14.5) vs. 13.7% (11.2–20.3), $p = 0.037$] but no statistically significant alteration was observed in NAWM DVR values (Fig. 3A-B; Table 2).

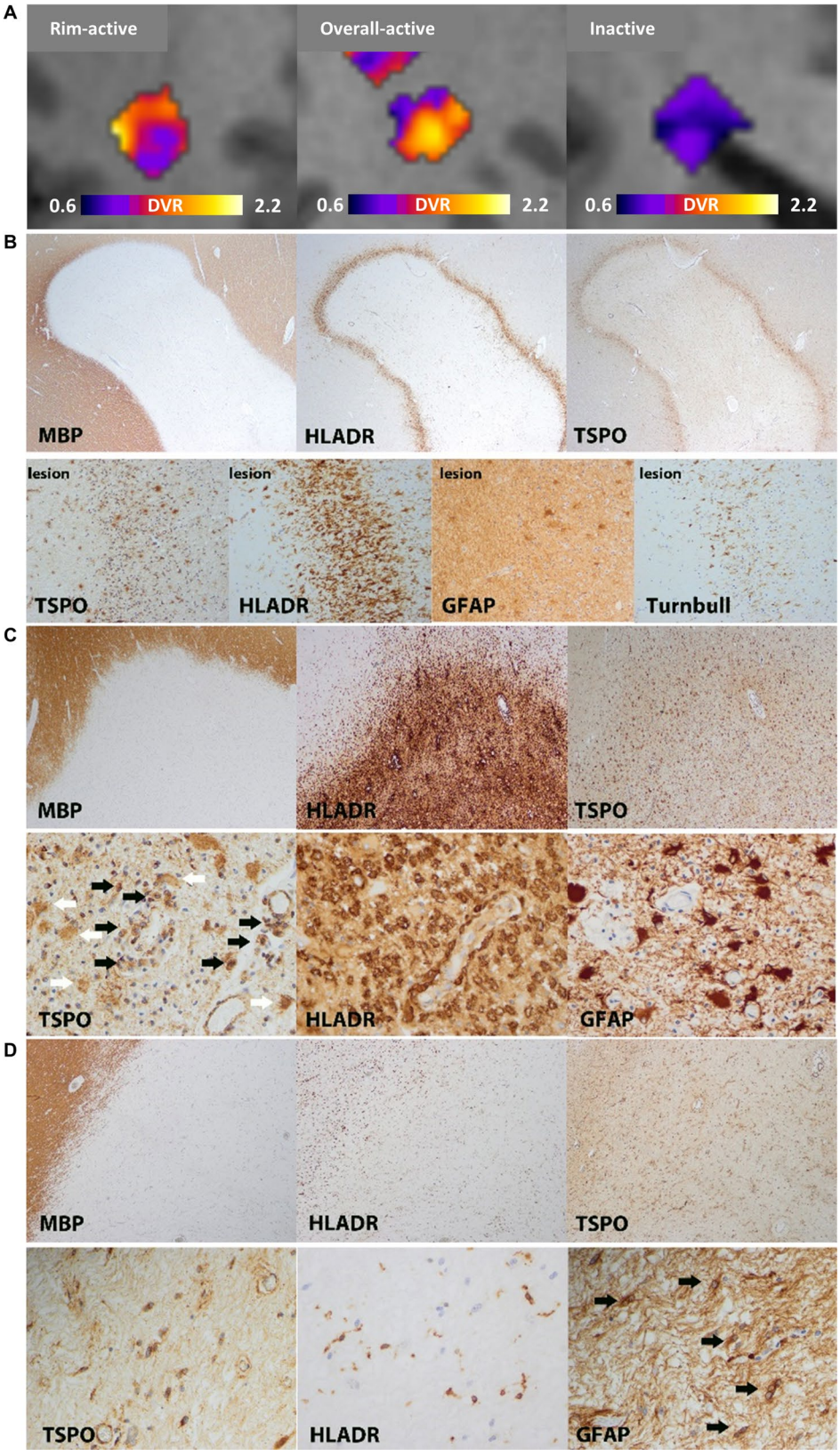

Fig. 2 (See legend on next page.)

(See figure on previous page.)

Fig. 2 Examples of chronic lesion phenotypes based on TSPO-PET and postmortem neuropathological immunohistochemical staining. **A**) An automated TSPO-PET-based method classifies lesions into rim-active, overall-active, and inactive categories based on the proportion of active voxels in the perilesional rim relative to the lesion core. **B**) The upper panel provides an overview of a mixed active/inactive lesion with a complete loss of MBP-positive myelin sheaths and a prominent rim of HLA-DR and TSPO positive microglia, likely corresponding to a TSPO-rim-active lesion. The lower panel shows higher magnifications of the rim stained for TSPO, HLA-DR and GFAP. GFAP staining shows strong fiber gliosis inside and outside of the lesion and single GFAP positive astrocytes at the rim. Turnbull staining demonstrates the presence of iron positive myeloid cells at the rim. **C**) The upper panel displays a completely demyelinated active lesion with a dense myeloid cell infiltrate (immunohistochemistry for MBP and HLA-DR). Within the active lesion, numerous TSPO positive cells are present. The lower panel shows higher magnifications of the immunohistochemical stainings demonstrating the presence of TSPO-expressing myeloid cells (black arrows) and astrocytes (white arrows). **D**) The upper panel depicts a completely demyelinated hypocellular inactive lesions with low numbers of HLA-DR positive myeloid cells that shows some TSPO-immunopositivity. Higher magnifications in the lower panel suggest that also GFAP-positive astrocytes express TSPO in inactive lesion. The inactive lesion shows a strong GFAP positive fiber gliosis, GFAP positive astrocytes are indicated by black arrows

Not correcting for other demographic characteristics, the baseline PET DVR or the change in PET DVR in the NAWM or at the perilesional area did not significantly associate with age (≤ 45 years of age; $n = 9$ vs. > 45 years of age; $n = 9$) or with previous relapse activity (relapse within past 4 years; $n = 8$ vs. relapse over four years ago; $n = 10$) (data not shown).

Changes in TSPO-PET based chronic lesion phenotypes during the one-year follow-up

This longitudinal study allowed us to explore the fate of chronic lesion phenotypes over the one-year follow-up period. Two patients with RRMS and four patients with SPMS had individual T1 hypointense lesions at baseline that fused into a confluent lesion during the one-year follow-up. The individual lesions in the baseline image were combined into one cohesive lesion for purposes of phenotyping. Seven out of eight of these cohesive lesions were phenotyped as overall-active lesions, and they retained this phenotype during the follow-up. One was phenotyped as rim-active and changed to overall-active during the one-year follow-up. A total of 36/216 lesions (17% of all inactive or overall active lesions at baseline, median 3, interquartile range IQR 2-3.75) evolved into a rim-active phenotype among SPMS patients, whereas only 9/124 lesions (7%, median 1, IQR 0–1) acquired a rim-active status among the RRMS cohort ($p = 0.016$, Fig. 3C). The number and volume of inactive lesions changing into rim-active lesions were significantly higher among SPMS compared to RRMS (Table 3), while other lesion changes were similar among the cohorts.

Three SPMS patients developed one new demyelinated white matter lesion during the one-year follow-up, two of which were small (< 50 voxels) inactive lesions and one was a small rim-active lesion. One RRMS patient developed two new overall active lesions, with no new clinical symptoms.

Baseline TSPO-binding associates with changes in volumetric and clinical measures during both one-year follow-up and 4–11-year extended follow-up

MR images from 13 patients and EDSS assessments from all 18 patients were available at the extended follow-up 4–11 years (average 7 years) after baseline for long-term atrophy and progression evaluation (Table 4). Eleven patients experienced confirmed disability progression and all demonstrated development of brain atrophy [mean annualized PBVC − 0.61 (± 0.57)] during the extended follow-up. Five patients (three with later MRI available) had started disease modifying therapy (rituximab, natalizumab or glatiramer acetate) approximately 2.1 years after baseline. Three of these patients had already progressed prior to treatment initiation and two did not have clinical progression during the extended follow-up.

Baseline TSPO DVRs associated with volumetric changes. A higher baseline TSPO DVR in the NAWM associated with greater reduction of cortical GM volume during the one-year follow-up (R = -0.48, $p = 0.048$, data not shown). Additionally, higher TSPO DVR in the thalamus at baseline correlated significantly with a greater brain volume reduction over the extended follow-up of 4–11 years measured as annualized PBVC (R = -0.59, $p = 0.036$, Supplementary Table 2). Other TSPO DVR values at baseline had no significant associations with brain volume changes after the one-year or extended 4–11-year follow-ups.

Baseline perilesional DVR but not NAWM DVR correlated significantly with EDSS change during the one-year follow-up ($R = 0.5$, $p = 0.036$, Fig. 4C) and during the extended 4–11-year ($R = 0.56$, $p = 0.016$, Fig. 4G) follow-up. Baseline DVR-values in T1 and T2 lesions correlated with EDSS change during the one-year follow-up ($R = 0.52$, $p = 0.028$ and $R = 0.47$, $p = 0.046$, respectively, data not shown). TSPO DVR values in other brain regions at baseline did not correlate significantly with EDSS increase over the one-year or the extended 4–11-year follow-ups.

There were six patients (2 RRMS and 4 SPMS) who experienced confirmed disability worsening during the

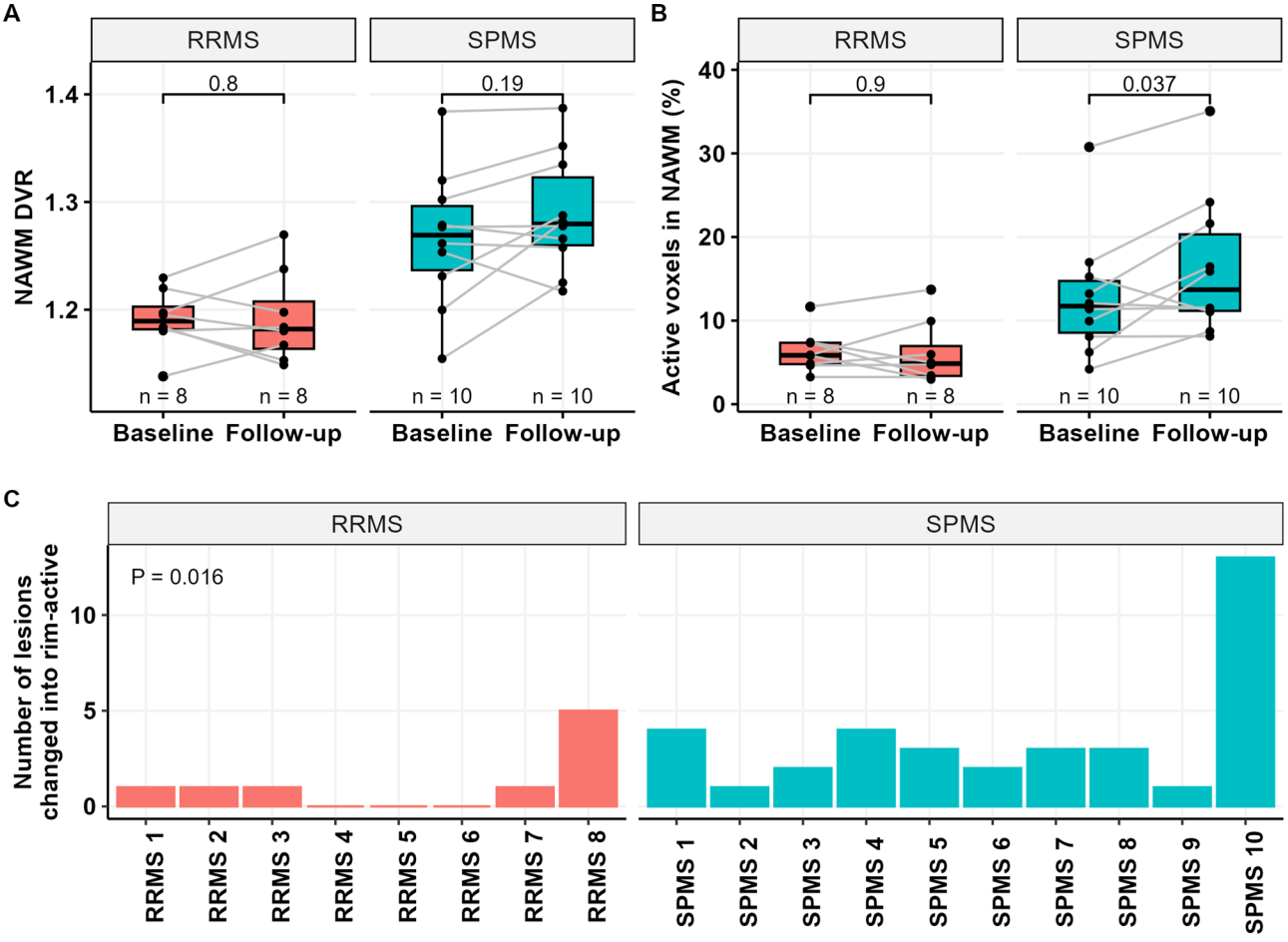

Fig. 3 Longitudinal changes in TSPO-binding among RRMS and SPMS patients over the one-year follow-up. No significant change was observed in NAWM DVR-values during the one-year follow-up among RRMS or SPMS patients (**A**). Among SPMS patients the proportion of active voxels increased significantly in the NAWM, which indicates an enhancement in glial activation during the observation period (**B**). SPMS patients had significantly more lesions that evolved into rim-active phenotype during the one-year follow-up compared to RRMS (**C**). Statistical analyses were performed with Wilcoxon signed-rank test (**A**-**B**) and Wilcoxon rank-sum test (**C**)

one-year follow-up and eleven patients (3 RRMS and 8 SPMS) who experienced confirmed disability worsening during the extended follow-up of 4–11 years. Those who progressed during the one-year follow-up had higher perilesional DVR at baseline compared to those who did not progress [mean (SD) 1.27 (0.08) vs. 1.18 (0.08), $p = 0.041$, Fig. 4D], and those who progressed during the extended 4–11-year follow-up had higher NAWM DVR at the baseline compared to those who did not progress [1.26 (0.07) vs. 1.19 (0.03), $p = 0.027$, Fig. 4F).

Greater change in TSPO-binding over the one-year follow-up predicts brain atrophy after 4–11-year extended follow-up

Patients with a greater increase in the proportion of active voxels in the NAWM or in the whole brain over the one-year follow-up had significantly greater reduction in brain volume measured after extended follow-up as annualized PBVC (R = -0.81, $p = 0.001$ and R = -0.73, $p = 0.007$, respectively, Fig. 5A-B, Supplementary Table 2). Similar association was observed with increased DVR values in these ROIs (Fig. 5C-D Supplementary Table 2). Additionally, greater increases in the cortical GM, T1 and T2 lesion DVRs during the one-year follow-up correlated significantly negatively with the annualized PBVC (R = -0.79, $p = 0.002$; R = -0.73, $p = 0.006$; R = -0.68, $p = 0.013$, respectively, Supplementary Table 2).

Linear regression model was used to analyse the associations between imaging parameters, demographic variables and later atrophy among the 13 patients with extended MRI follow-up (Supplementary Table 2). The imaging parameters which demonstrated significant Spearman correlation with annualized PBVC included thalamus DVR at baseline, and change from baseline to one year in the following variables: brain DVR, NAWM DVR, T1 lesion DVR, T2 lesion DVR, proportion of active voxels in the brain, proportion of active voxels in NAWM, and T2 lesion volume.

Table 3 TSPO-PET based chronic lesion phenotypes at baseline and during follow-up

		Inactive to rim-active	Overall-active to rim-active	Overall-active to inactive	Rim-active to inactive	Inactive to overall-active	Rim-active to overall-active
Number of lesions (patient level)	RRMS 1	0	1	3	0	0	2
	RRMS 2	0	1	4	4	1	0
	RRMS 3	1	0	4	2	0	3
	RRMS 4	0	0	0	0	0	0
	RRMS 5	0	0	1	2	3	0
	RRMS 6	0	0	2	0	2	0
	RRMS 7	0	1	0	0	2	1
	RRMS 8	1	4	1	1	5	2
	SPMS 1	2	2	0	0	0	2
	SPMS 2	1	0	0	0	2	0
	SPMS 3	2	0	2	0	2	3
	SPMS 4	0	4	2	2	0	2
	SPMS 5	1	2	3	3	3	1
	SPMS 6	1	1	1	0	0	4
	SPMS 7	1	2	0	2	0	0
	SPMS 8	3	0	4	0	3	0
	SPMS 9	0	1	0	0	0	3
	SPMS 10	6	7	2	1	11	2
Number of lesions (cohort level)	RRMS, median (IQR)	0 (0-0.25)	0.5 (0–1)	1.5 (0.75–3.25)	0.5 (0–2)	1.5 (0–2)	0.5 (0–2)
	SPMS, median (IQR)	1 (1–2)	1.5 (0.25-2)	1.5 (0–2)	0 (0-1.75)	1 (0-2.75)	2 (0.25–2.75)
	p-value*	**0.015**	0.2	0.6	0.7	0.9	0.3
Volume of lesions (cohort level)	RRMS, median (IQR)	0 (0–8)	16 (0-110)	204 (28–476)	17 (0-105)	112 (0-291)	37 (0-246)
	SPMS, median (IQR)	51 (30–107)	54 (8-170)	186 (0-304)	0 (0–62)	43 (0-182)	212 (15–365)
	p-value*	**0.036**	0.4	0.7	0.6	0.7	0.4

*Wilcoxon rank-sum test. If two or more lesions grew and fused into a single confluent lesion during the follow-up, the baseline phenotype was determined by combining the corresponding individual lesions into one cohesive lesion. IQR = Interquartile range, RRMS = Relapsing remitting multiple sclerosis, SPMS = Secondary progressive multiple sclerosis

Table 4 Longitudinal disability and atrophy outcomes

	Baseline		4–11-year extended follow-up		Baseline vs. 4–11-year extended follow-up
Clinical outcome, n = 18	**Median**	**IQR**	**Median**	**IQR**	***p-value***
EDSS	3.8	3.0–6.0	5.0	3.5–6.4	**0.019**
MRI volumetric outcomes, n = 13	**Mean**	**SD**	**Mean**	**SD**	***p-value***
Brain volume, cm^3	1132	170	1105	166	**0.013**
WM volume, cm^3	554	386	546	384	0.133
Cortical GM volume, cm^3	430	54	402	59	**0.001**
Thalamus volume, cm^3	13	2.3	12	2.3	0.173

EDSS = Expanded Disability Status Scale, IQR = Interquartile range, MRI = magnetic resonance imaging, WM = White matter, GM = Gray matter

Forward-type stepwise multiple linear regression was performed to identify significant predictors for annualized PBVC. The final model, with–log(–(annualized PBVC)) as the outcome, included the change in the proportion of active voxels in the NAWM ($p = 0.004$) and baseline BMI ($p = 0.067$) as the best predictors (Fig. 5E). The R^2 value of the model including only the change in the proportion of active voxels in the NAWM over the one-year follow-up as a predictor was 55%, indicating that this variable accounted for over the half of the variance in later brain atrophy. Adding the baseline BMI to the model increased the R^2 to 69% suggesting that the combination of the two predictors explain a substantial proportion of the variance in later brain atrophy development.

Discussion

We demonstrate in this work an increase in TSPO-PET-signal in the NAWM among untreated SPMS but not RRMS patients over the one-year follow-up. We furthermore show that the increase in TSPO-binding in the NAWM over the one-year follow-up predicts later adverse outcomes manifested by brain atrophy development. Additionally, we confirm that higher

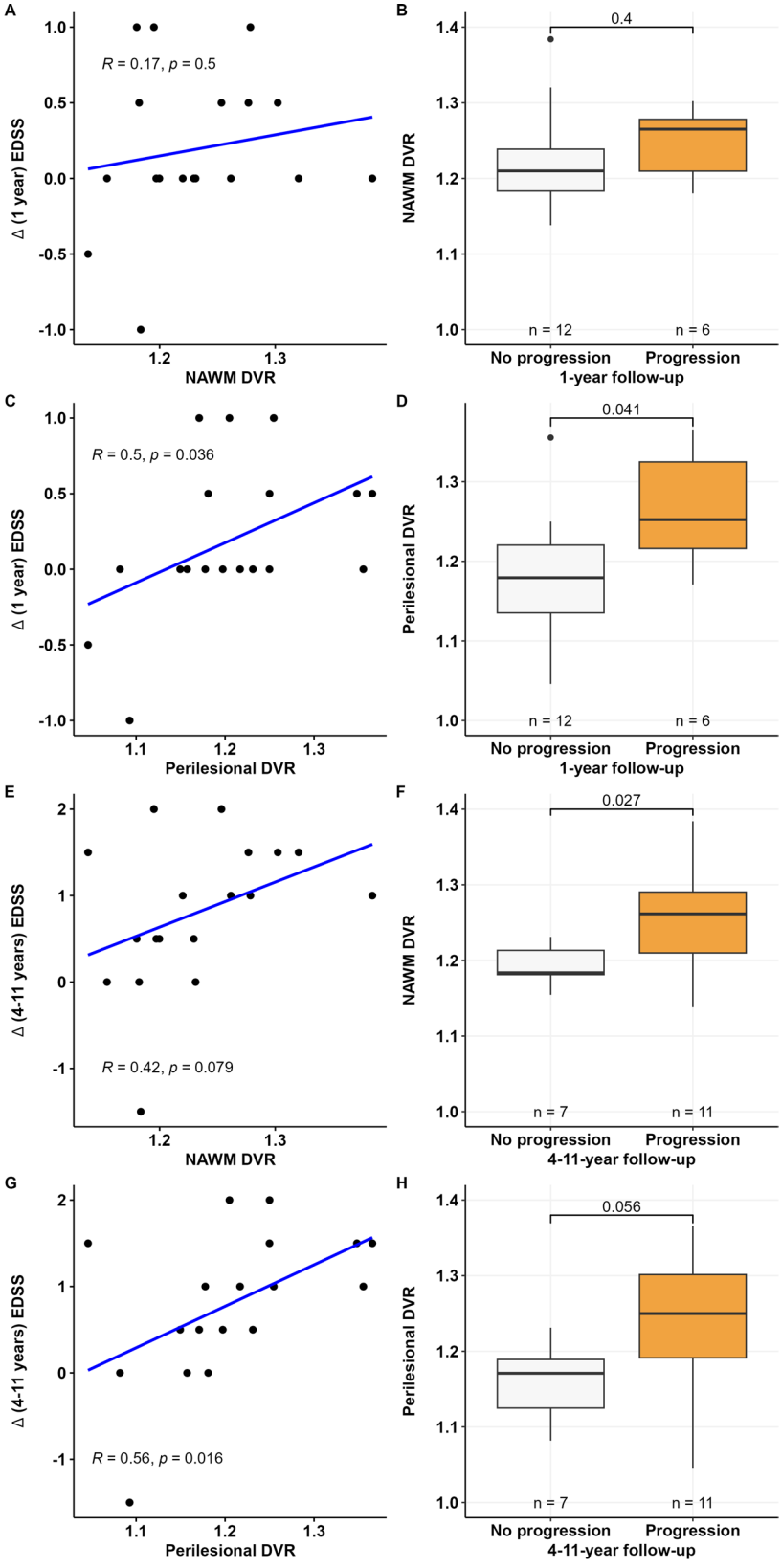

Fig. 4 (See legend on next page.)

(See figure on previous page.)

Fig. 4 Baseline TSPO-binding associates with later clinical progression. Higher DVR at the perilesional area at baseline associated with greater EDSS increase during both one-year (**C**) and the extended 4–11-year follow-up periods (**G**). The associations between a greater baseline NAWM DVR and EDSS increase during either follow-up period were not significant (**A** and **E**). Patients with confirmed disability progression during the one-year follow-up had greater TSPO-binding (DVR) at the perilesional area but not in the NAWM compared to stable patients (**B** and **D**). Patients with confirmed disability progression during the extended 4–11-year follow-up had greater TSPO-binding (DVR) in the NAWM but not at the perilesional area compared to stable patients (F and H). Statistical analyses were performed with Spearman correlation and Wilcoxon rank-sum test

TSPO-binding at baseline is associated with later clinical disability progression after both short-term (one-year) and extended (4–11-year) time periods. These findings are the first to demonstrate natural evolution in CNS-compartmentalized glial activation in clinically distinct MS cohorts. The strong association between the increase in TSPO-signal over one year and later development of brain atrophy supports the concept of harmful smoldering inflammation.

Neuropathological studies give a detailed snapshot of the cellular phenotypes associated with MS pathology at various disease stages [6, 25], but TSPO-PET-imaging can be used to capture the presence and dynamic evolution of glial activation in vivo. Longitudinal TSPO-PET-imaging has demonstrated either a reduction [13, 14, 26, 27] or no alteration [20] in TSPO-radioligand availability following treatments but present work is the first demonstration of an increase in TSPO-binding among untreated SPMS but not RRMS patients over the one-year prospective follow-up. This increase in TSPO-binding among SPMS patients was observed not only in the NAWM but also in relation to chronic lesions, as inactive lesions were shown to acquire rim-activity.

Despite the comparable disease duration and age of the cohorts, the SPMS cohort comprised a clearly more advanced group of MS patients with high EDSS, significant lesion volume and increased TSPO-binding, while the RRMS cohort represented a more benign group of patients with low EDSS and low lesion volume. The differences in the level of CNS-compartmentalized inflammation both in a cross-sectional setting and longitudinally in these two cohorts, highlights the importance of both diffuse and lesion-associated innate immune cell activation for MS disease progression. While the differences in the level and evolution of TSPO-availability in the now studied RRMS and SPMS cohorts were quite pronounced, we do not doubt the existence of RRMS patients who demonstrate significantly higher TSPO-binding and greater proportions of rim-active chronic lesions already in early disease, and who thereby would benefit of treatments targeting CNS-contained innate immune cell activation.

The increase in TSPO-availability in the NAWM over the one-year follow-up was associated with more pronounced brain atrophy measures after 4–11 years. According to multiple linear regression modelling, the change in the proportion of active voxels in the NAWM was the best predictor for later atrophy development. Importantly, all significant disease-associated and demographic variables were also tested in the model predicting later atrophy. Of all tested variables the only significant parameter surviving in the model was the increase in inflammatory burden in the CNS measured as an increase in TSPO-binding. Although baseline BMI was included in the model and higher BMI has been previously associated with greater brain atrophy [28] and lower TSPO-binding [29] among healthy controls, it was not significantly associated with TSPO-binding or brain atrophy in this cohort.

While the majority of the increased TSPO-PET-signal originates from pathologically increased density of activated microglia and macrophages, a proportion of the signal comes from astrocytes [30]. Therefore, the determination of the exact cellular sources of the TSPO-signal is challenging in the context of clinical imaging. Particularly among the TSPO overall-active lesions, the increased TSPO-binding in the core and at rim could reflect either microglia and macrophage activation related to a relatively recently evolved active lesion, but the signal could also reflect reactive astrogliosis or glial scar formation [6]. Based on the staining data demonstrating TSPO co-localization with activated microglia at the rim of mixed-active/inactive lesion, and the high TSPO-binding at the chronic lesion edge at imaging, we are tempted to interpret that the increased signal associated with chronic lesion edge reflects mainly the proinflammatory innate immune cell activation.

There are some limitations to this study. The studied patient number is relatively small, but in the present day most MS patients in developed countries are treated and hence in vivo evaluation of natural pathology evolution using advanced imaging is becoming more challenging. In addition, the lack of inclusion of susceptibility-weighted sequences in the MRI protocol prevented us from addressing the impact of paramagnetic lesions on disease evolution in these untreated cohorts and can be considered a limitation of the study.

Glial cell activation seems a remarkably important pathological determinant which promotes neurodegenerative processes resulting with brain atrophy and clinical disease progression. Reversing pro-inflammatory innate immune cell activation may be beneficial for slowing down disease progression, and microglia-associated inflammation is being currently investigated as a therapeutic target in progressive

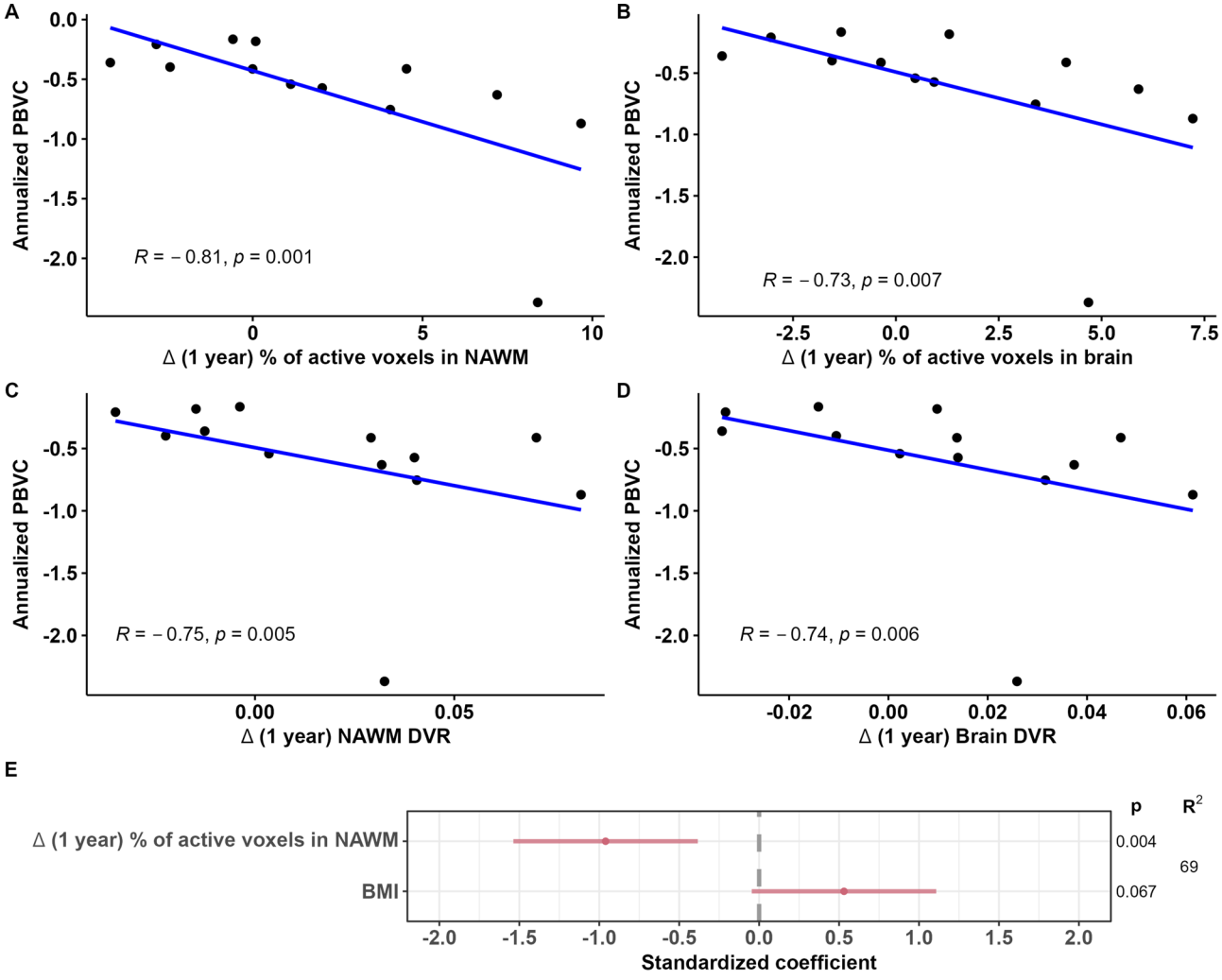

Fig. 5 A greater increase in TSPO-binding during the one-year follow-up associates with more pronounced brain atrophy outcome over 4–11 years. A greater increase in the TSPO-binding in the NAWM and whole brain during the one-year follow-up associate with later brain atrophy measured as annualized PBVC (**A**-**D**). According to multiple linear regression modelling the increase in active voxels in the NAWM and baseline BMI explain 69% of the variance in later brain atrophy (**E**). Statistical analyses were performed with Spearman correlation (**A**-**D**) and multiple linear regression (**E**)

MS [12]. While iron-sensitive MRI-sequences can be used to identify a subset of chronic active lesions [4], TSPO-PET-imaging is presently the only applicable in vivo tool to detect dynamic longitudinal changes in glial activation within the CNS [14, 20].

Abbreviations

AIC	Akaike information criterion
ARR	Annualized relapse rate
BMI	Body mass index
CNS	Central nervous system
DAB	Diaminobenzidine
DMT	Disease modifying treatment
DVR	Distribution volume ratio
EDSS	Expanded disability status scale
FLAIR	Fluid-attenuated inversion recovery
GFAP	Glial fibrillary acidic protein
GM	Grey matter
HC	Healthy control
HLA-DR	Human leukocyte antigen
HRRT	High-resolution research tomograph
ICV	Intracranial volume
IQR	Interquartile range
MBP	Myelin basic protein
MRI	Magnetic resonance imaging
MS	Multiple sclerosis
NAWM	Normal appearing white matter
PBS	Phosphate-buffered saline
PBVC	Percentage brain volume change
PET	Positron emission tomography
ROI	Region of interest
RRMS	Relapsing remitting multiple sclerosis
SD	Standard deviation
SPMS	Secondary progressive multiple sclerosis
TSPO	18-kDa translocator protein
WM	White matter

Supplementary Information

The online version contains supplementary material available at https://doi.org/10.1186/s12974-025-03519-y.

Supplementary Material 1

Acknowledgements
All the study participants and the expert staff at Turku PET Centre are gratefully acknowledged for making this study possible. Luisa Klotz, Amelie Luoma, Anna Vuorimaa, Eero Rissanen, Eveliina Honkonen, Mikko Koivumäki and Sini Laaksonen are acknowledged for their valuable input in this study.

Author contributions
MN, JL, MS and LA contributed to the study conception and design. MN, JL, MM, JR, SW, MS and TK contributed to data acquisition and analysis. MN, JL, MM, MS, TK and LA contributed to the interpretation of data. MN, JL, MM, TK and LA drafted the work or substantively revised. All authors read and approved the final manuscript.

Funding
This work was financially supported by the Finnish Cultural Foundation (MN), University of Turku Drug Research Doctoral Programme (MN), The Finnish MS Foundation (MN), the Research Council of Finland's Flagship InFLAMES (decision numbers 337530, 357910 and 358823) (MN, JL, LA), the Research Council of Finland (decision number 330902) (LA), Jane and Aatos Erkko foundation (#220026) (LA), National MS Society and the National Stem Cell Foundation (RFA-2203-39281) (LA).

Data availability
The data used in the preparation of this article is not publicly available due to the protection of patients' privacy. Anonymized raw PET data is available from the corresponding author on reasonable request.

Declarations

Competing interests
The authors declare no competing interests.

Human ethics and consent to participate
The study protocol was approved by the Ethics Committee of the Hospital District of Southwest Finland (Dnro:76/180/2008 and Dnro:86/1800/2017). Written informed consent was obtained from all participants according to the principles of the Declaration of Helsinki. The study for postmortem neuropathological staining was approved by the Ethics Committee of the University of Münster (Ref: 2011-153-f-S).

Author details
[1]Turku PET Centre, University of Turku, Turku University Hospital and Åbo Akademi University, Turku, Finland
[2]InFLAMES Research Flagship, University of Turku, Turku, Finland
[3]Clinical Neurosciences, University of Turku, Turku, Finland
[4]Neurocenter, Turku University Hospital, Turku, Finland
[5]Åbo Akademi University, Turku, Finland
[6]Institute of Neuropathology, University Hospital Münster, Münster, Germany

Received: 11 April 2025 / Accepted: 15 July 2025
Published online: 07 August 2025

References

1. Miller DH, Hornabrook RW, Purdie G. The natural history of multiple sclerosis: a regional study with some longitudinal data. Neurosurgery, and Psychiatry. 1992;55:341–6. Available from: https://doi.org/10.1136/jnnp.55.5.341
2. Reich DS, Lucchinetti CF, Calabresi PA. Multiple Sclerosis. New England Journal of Medicine. 2018;378:169–80. Available from: https://www.nejm.org/doi/full/10.1056/NEJMra1401483
3. Giovannoni G, Popescu V, Wuerfel J, Hellwig K, Iacobeus E, Jensen MB et al. Smouldering multiple sclerosis: the 'real MS.' Ther Adv Neurol Disord. 2022;15. Available from: https://journals.sagepub.com/doi/10.1177/17562864211066751
4. Bagnato F, Sati P, Hemond CC, Elliott C, Gauthier SA, Harrison DM et al. Imaging chronic active lesions in multiple sclerosis: a consensus statement. Brain. 2024;27. Available from: https://doi.org/10.1093/brain/awae013
5. Hamzaoui M, Garcia J, Boffa G, Lazzarotto A, Absinta M, Ricigliano VAG et al. Positron Emission Tomography with [18F]-DPA-714 Unveils a Smoldering Component in Most Multiple Sclerosis Lesions which Drives Disease Progression. Ann Neurol. 2023;94:366–83. Available from: https://doi.org/10.1002/ana.26657
6. Kuhlmann T, Ludwin S, Prat A, Antel J, Brück W, Lassmann H. An updated histological classification system for multiple sclerosis lesions. Acta Neuropathol. 2017;133:13–24. Available from: https://link.springer.com/article/10.1007/s00401-016-1653-y
7. Klotz L, Smolders J, Lehto J, Matilainen M, Lütje L, Buchholz L et al. Broad rim lesions are a new pathological and imaging biomarker for rapid disease progression in multiple sclerosis. Nat Med. 2025;14:1–11. Available from: https://www.nature.com/articles/s41591-025-03625-7
8. Chauveau F, Becker G, Boutin H. Have (R)-[11 C]PK11195 challengers fulfilled the promise? A scoping review of clinical TSPO PET studies. Eur J Nucl Med Mol Imaging. 2021;49:201–20. Available from: https://link.springer.com/article/10.1007/s00259-021-05425-w
9. Sucksdorff M, Matilainen M, Tuisku J, Polvinen E, Vuorimaa A, Rokka J et al. Brain TSPO-PET predicts later disease progression independent of relapses in multiple sclerosis. Brain. 2020;143:3318–30. Available from: https://doi.org/10.1093/brain/awaa275
10. Misin O, Matilainen M, Nylund M, Honkonen E, Rissanen E, Sucksdorff M et al. Innate Immune Cell-Related Pathology in the Thalamus Signals a Risk for Disability Progression in Multiple Sclerosis. Neurol Neuroimmunol Neuroinflamm. 2022;9. Available from: https://doi.org/10.1212/NXI.0000000000001182
11. Polvinen E, Matilainen M, Nylund M, Sucksdorff M, Airas LM. TSPO-Detectable Chronic Active Lesions Predict Disease Progression in Multiple Sclerosis. Neurology(R) neuroimmunology & neuroinflammation. 2023;10. Available from: https://doi.org/10.1212/NXI.0000000000200133
12. Airas L, Yong VW. Microglia in multiple sclerosis - Pathogenesis and imaging. Curr Opin Neurol. 2022;35:299–306. Available from: https://journals.lww.com/co-neurology/fulltext/2022/06000/microglia_in_multiple_sclerosis___pathogenesis_and.8.aspx
13. Lehto J, Sucksdorff M, Nylund M, Raitanen R, Matilainen M, Airas L. PET-measurable innate immune cell activation reduction in chronic active lesions in PPMS brain after rituximab treatment: a case report. J Neurol. 2023;270:2329–32. Available from: https://link.springer.com/article/10.1007/s00415-022-11539-4
14. Sucksdorff M, Tuisku J, Matilainen M, Vuorimaa A, Smith S, Keitilä J et al. Natalizumab treatment reduces microglial activation in the white matter of the MS brain. Neurol Neuroimmunol Neuroinflamm. 2019;6. Available from: https://doi.org/10.1212/NXI.0000000000000574
15. Kalincik T, Cutter G, Spelman T, Jokubaitis V, Havrdova E, Horakova D et al. Defining reliable disability outcomes in multiple sclerosis. Brain. 2015;138:3287–98. Available from: https://doi.org/10.1093/brain/awv258
16. Schmidt P, Gaser C, Arsic M, Buck D, Förschler A, Berthele A et al. An automated tool for detection of FLAIR-hyperintense white-matter lesions in Multiple Sclerosis. Neuroimage. 2012;59:3774–83. Available from: https://doi.org/10.1016/j.neuroimage.2011.11.032
17. Nylund M, Sucksdorff M, Matilainen M, Polvinen E, Tuisku J, Airas L. Phenotyping of multiple sclerosis lesions according to innate immune cell activation using 18 kDa translocator protein-PET. Brain Commun. 2022;4. Available from: https://doi.org/10.1093/braincomms/fcab301
18. Smith SM, Zhang Y, Jenkinson M, Chen J, Matthews PM, Federico A et al. Accurate, Robust, and Automated Longitudinal and Cross-Sectional Brain Change Analysis. Neuroimage. 2002;17:479–89. Available from: https://doi.org/10.1006/nimg.2002.1040
19. Smith SM, Jenkinson M, Woolrich MW, Beckmann CF, Behrens TEJ, Johansen-Berg H et al. Advances in functional and structural MR image analysis and implementation as FSL. Neuroimage. 2004;23:S208–19. Available from: https://doi.org/10.1016/j.neuroimage.2004.07.051
20. Lehto J, Nylund M, Matilainen M, Sucksdorff M, Vuorimaa A, Rajander J et al. Longitudinal stability of progression-related microglial activity during teriflunomide treatment in patients with multiple sclerosis. Eur J Neurol. 2023;30:2365–75. Available from: https://onlinelibrary.wiley.com/doi/full/10.1111/ene.15834
21. Alakurtti K, Aalto S, Johansson JJ, Någren K, Tuokkola T, Oikonen V et al. Reproducibility of striatal and thalamic dopamine D2 receptor binding using 11 Craclopride with high-resolution positron emission tomography. Journal of Cerebral Blood Flow and Metabolism. 2011;31:155–65. Available from: https://doi.org/10.1038/jcbfm.2010.64
22. Logan J, Fowler JS, Volkow ND, Wang G-J, Ding Y-S, Alexoff DL. Distribution Volume Ratios without Blood Sampling from Graphical Analysis of PET Data.

Journal of Cerebral Blood Flow & Metabolism. 1996;16:834–40. Available from: https://doi.org/10.1097/00004647-199609000-00008
23. Meguro R, Asano Y, Odagiri S, Li C, Iwatsuki H, Shoumura K. Nonheme-iron histochemistry for light and electron microscopy: a historical, theoretical and technical review. Arch Histol Cytol. 2007;70:1–19. Available from: https://doi.org/10.1679/aohc.70.1
24. Gelman A. Scaling regression inputs by dividing by two standard deviations. Stat Med. 2008;27:2865–73. Available from: https://doi.org/10.1002/sim.3107
25. Frischer JM, Weigand SD, Guo Y, Kale N, Parisi JE, Pirko I et al. Clinical and pathological insights into the dynamic nature of the white matter multiple sclerosis plaque. Ann Neurol. 2015;78:710–21. Available from: https://onlinelibrary.wiley.com/doi/full/10.1002/ana.24497
26. Kaunzner UW, Kang Y, Monohan E, Kothari PJ, Nealon N, Perumal J et al. Reduction of PK11195 uptake observed in multiple sclerosis lesions after natalizumab initiation. Mult Scler Relat Disord. 2017;15:27–33. Available from: https://doi.org/10.1016/j.msard.2017.04.008
27. Ratchford JN, Endres CJ, Hammoud DA, Pomper MG, Shiee N, McGready J et al. Decreased microglial activation in MS patients treated with glatiramer acetate. J Neurol. 2011;259:1199. Available from: https://doi.org/10.1007/s00415-011-6337-x
28. Ward MA, Carlsson CM, Trivedi MA, Sager MA, Johnson SC. The effect of body mass index on global brain volume in middle-aged adults: A cross sectional study. BMC Neurol. 2005;5:1–7. Available from: https://bmcneurol.biomedcentral.com/articles/10.1186/1471-2377-5-23
29. Tuisku J, Plavén-Sigray P, Gaiser EC, Airas L, Al-Abdulrasul H, Brück A et al. Effects of age, BMI and sex on the glial cell marker TSPO — a multicentre [11 C]PBR28 HRRT PET study. Eur J Nucl Med Mol Imaging. 2019;46:2329–38. Available from: https://link.springer.com/10.1007/s00259-019-04403-7
30. Nutma E, Stephenson JA, Gorter RP, De Bruin J, Boucherie DM, Donat CK et al. A quantitative neuropathological assessment of translocator protein expression in multiple sclerosis. Brain. 2019;142:3440–55. Available from: https://doi.org/10.1093/brain/awz287

Publisher's note